THE ASTROPHYSICAL JOURNAL, 452:588–598, 1995 October 20

UPPER LIMITS ON TeV GAMMA-RAY EMISSION FROM ACTIVE GALACTIC NUCLEI

A. D. KERRICK,[1,2] C. W. AKERLOF,[3] S. BILLER,[4] J. BUCKLEY,[5] D. A. CARTER-LEWIS,[1] M. F. CAWLEY,[6] M. CHANTELL,[5] V. CONNAUGHTON,[5,7] D. J. FEGAN,[7] S. FENNELL,[7] J. GAIDOS,[8] A. M. HILLAS,[4] P. W. KWOK,[1,9] R. C. LAMB,[1] T. LAPPIN,[5] R. LESSARD,[7] J. MCENERY,[7] D. I. MEYER,[3] G. MOHANTY,[1] J. QUINN,[7] H. J. ROSE,[4] A. C. ROVERO,[5,10] G. SEMBROSKI,[8] M. S. SCHUBNELL,[3] M. PUNCH,[7,11] T. C. WEEKES,[5] M. WEST,[4] C. WILSON,[8] AND J. ZWEERINK[1]

Received 1995 January 27; accepted 1995 May 2

ABSTRACT

The results of a search for TeV gamma-ray emission from 35 active galactic nuclei (AGNs) using the Whipple Observatory High Resolution Atmospheric Cerenkov Camera are reported. Fifteen of these objects have been detected at GeV energies by the EGRET experiment on the *Compton Gamma Ray Observatory*. None of the 35 objects gave a signal at the 3 σ level; Mrk 421 remains the only AGN detected at TeV energies. The absence of a TeV signal may imply a change in the primary source spectrum and/or the effect of absorption by pair production on intergalactic infrared photons.

Subject headings: galaxies: active — galaxies: nuclei — gamma rays: observations

1. INTRODUCTION

The central engines of active galactic nuclei (AGNs) are presumed to be massive black holes whose accretion powers radiation over a wide range of the electromagnetic spectrum. The high energy output, the short time variations, the optical polarization, and the emission of X-rays strongly hint at the presence of high-energy particle acceleration and interaction within these objects; however, until recently there was no direct evidence for cosmic-ray production there. The detection of MeV-GeV gamma rays from 42 AGNs by the EGRET experiment on the *Compton Gamma Ray Observatory* (Fichtel et al. 1994; von Montigny et al. 1995) has dramatically changed this picture and demonstrated clearly that at least at these energies the relativistic jets are particle beams. The detection of TeV gamma rays from the nearby AGN Mrk 421 (Punch et al. 1992) is an indication that the particle acceleration is not limited to GeV energies and that the AGNs may be true cosmic particle accelerators.

The detection of a physical cutoff in the detected emission spectrum at these energies may be an important clue to the emission mechanisms in the relativistic jets; hence, it is important to establish the energy spectrum at energies of 100 GeV and beyond. These are the energies accessible to the ground-based atmospheric Cerenkov technique; as has been demonstrated by the detection of Mrk 421, these techniques have flux sensitivities that effectively complement that of EGRET for sources with flat spectra.

If many AGNs are found to be TeV emitters and the progenitor particles are hadrons, then these AGNs must be prodigious emitters of cosmic rays. Ultimately, observations of the EGRET-detected AGNs at TeV energies may force a reevaluation of the role of extragalactic sources in the production of the observed high-energy cosmic-ray flux.

Upper limits on AGNs were first reported by the Whipple Collaboration in 1985 based on observations made the previous year (Cawley et al. 1985); the objects selected for observation included 3C 273, 3C 279, and Mrk 421. Upper limits on AGNs from observations with first generation atmospheric Cerenkov systems have also been reported (Long et al. 1965; Weekes et al. 1972; Weekes 1973; Stepanian et al. 1975). A detection of Centaurus A was reported (Grindlay et al. 1975) but has not been confirmed. This paper reports on observations of AGNs in the epoch 1991–1994 after the discovery by EGRET of 3C 279 in its high state (Hartman et al. 1992). Observations of Mrk 421, the only object to give a consistent signal at TeV energies, are reported elsewhere (Schubnell et al. 1995).

2. IMAGING TECHNIQUE

The observations reported in this paper were made using the atmospheric Cerenkov imaging technique (Cawley & Weekes 1995); they were taken with the 10 m optical reflector located at the Whipple Observatory on Mount Hopkins in Arizona, at an elevation of 2.3 km and latitude of 31°41′N. A high-resolution camera, consisting of 109 photomultiplier tubes (PMTs), was mounted in the focal plane of the reflector and recorded images of atmospheric Cerenkov radiation produced by gamma rays and cosmic rays. The camera has been described in detail by Cawley et al. (1990). Initially it consisted of 91 2.5 cm PMTs in a hexagonal matrix with 0°.25 spacing between centers, along with an outer ring of 18 tubes. Later the outer ring of 5 cm tubes was replaced by a partial outer ring of

[1] Department of Physics and Astronomy, Iowa State University, Ames, IA 50011-3160.
[2] Postal address: Department of Physics and Geology, Northern Kentucky University, Highland Heights, KY 41099.
[3] Randall Laboratory of Physics, University of Michigan, Ann Arbor, MI 48109-1120.
[4] Department of Physics, University of Leeds, Leeds, LS2 9JT, Yorkshire, England, UK.
[5] Fred Lawrence Whipple Observatory, Harvard-Smithsonian Center for Astrophysics, P.O. Box 97, Amado, AZ 85645-0097.
[6] Physics Department, St. Patrick's College, Maynooth, County Kildare, Ireland.
[7] Physics Department, University College, Dublin, Ireland.
[8] Department of Physics, Purdue University, West Lafayette, IN 47907.
[9] Postal address: Department of Physics, University of Hong Kong, Hong Kong.
[10] Postal address: I.A.F.E., Casilla de Correo 67, Sucursal 28, 1428, Buenos Aires, Argentina.
[11] Postal address: LPNHE, Ecole Polytechnique, Palaiseau, France.

18 2.5 cm tubes, with three tubes centered along each side of the hexagon formed by the inner 91 tubes.

The basic observing technique and data analysis method was as described in Reynolds et al. (1993) although, as noted in §§ 3.2 and 4 below, a number of innovations were introduced.

3. OBSERVATIONS

3.1. *Choice of Candidate Source*

Following the successful detection by EGRET of 3C 279 (Hartman et al. 1992), the observation of AGNs was given high priority in the Whipple Observatory Collaboration gamma-ray observing program. The criteria for selection of an AGN as a candidate object to be observed in this program changed with time as more information on gamma-ray–emitting AGNs became available; generally the selection was based on some of the following criteria:

1. The position of the source was such that it can be observed near the zenith at the Whipple Observatory;
2. The AGN had been detected by EGRET;
3. The AGN was a blazar at low redshift;
4. The AGN was interesting for a variety of other reasons.

These criteria were only loosely applied, so that the actual observing list (which is limited also by weather and other observing constraints) is by no means complete.

The candidate sources are listed in Table 1 in order of right ascension together with their classification, their EGRET detection status, and their redshift (if known).

3.2. *Operating Settings*

The camera is triggered when N of the inner 91 tubes exceed a preset threshold of p photoelectrons in a time interval τ. When N is small, the camera preferentially triggers on gamma-ray showers because the angular extent of the Cerenkov images from electromagnetic cascades is smaller than that from hadronic cascades. This hardware discrimination is 90% effective; i.e., the triggering rate on background events is only 10% of that expected with a full field of 3°. The principal discrimination comes off-line when simulations are used to identify candidate gamma-ray images (see below).

At the beginning and end of each night's observations, calibration data are obtained using a fast nitrogen flash lamp to artificially trigger the camera to determine relative tube gains. After every tenth event the camera is also triggered to measure the electronic pedestals which are broadened by fluctuations in the brightness of the night sky.

The energy threshold of the camera was originally determined by simulations and is updated for new instrument conditions by assuming that the background count rate R scales with energy threshold T with the cosmic-ray background, i.e.,

TABLE 1

CANDIDATE SOURCES

Source	Class[a]	EGRET Detection?[b]	Redshift	Other Names
0116+319.....		U.L.	0.059	4C +31.04
0202+149.....	QSO	yes	N/A	4C +15.05, PKS
0219+428.....	BL, OVV		0.444	3C 66A
0232−090.....	Seyfert		0.042	NGC 095, Mrk 1048
0235+164.....	BL, OVV	yes	0.94	OD 160, PKS
0241+622.....	Seyfert		0.044	4U
0316+413.....	Seyfert		0.018	NGC 1275
0415+379A.....	Seyfert		0.049	3C 111
0431+29	Unidentified	yes	N/A	GRO J0431+29
0528+134.....	QSO	yes	2.06	OG +147
0716+714.....	BL, OVV	yes	N/A	
0836+710.....		yes	2.17	4C +71.07
0855+201.....	BL, OVV	U.L.	0.306	OJ 287, PKS
1022+519.....	Seyfert		0.045	Mrk 142
1156+295.....	OVV	U.L.[c]	0.729	4C +29.45
1208+396.....	Seyfert		0.003	NGC 4151
1215+303.....	BL, OVV	U.L.	0.237	ON 325
1219+285.....	BL, OVV	U.L.[c]	0.102	W Comae, ON 231
1222+216.....		Marg.[c]	0.435	4C +21.35, PKS
1226+023.....	OVV	yes	0.158	3C 273
1253−055.....	OVV	yes	0.538	3C 279
1353+388.....	Seyfert		0.051	Mrk 464
1400+162.....	BL, OVV	U.L.	0.244	4C +16.39, PKS
1514+072.....			0.034	3C 317, 4C +07.40, PKS
1604+159.....	BL	Marg.[c]	N/A	4C +15.54, PKS
1633+382.....	OVV	yes	1.81	4C +38.41
1652+398.....	BL	U.L.	0.033	Mrk 501
1720+309.....	Seyfert		0.043	Mrk 506
1727+502.....	BL, OVV	U.L.	0.055	I Zw 187
1837+59	GRO	yes	N/A	J1837+59
2022−077.....		yes[c]	N/A	202203−081515
2200+420.....	BL, OVV	U.L.	0.069	BL Lac
2230+114.....	OVV	yes	1.037	CTA 102, PKS
2251+158.....	OVV	yes	0.859	3C 454.3, 4C +15.76
2304+042.....	Seyfert		0.042	PG

[a] "BL" = BL Lac object; "OVV" = optically violent variable.
[b] "Marg." = marginal detection; "U.L." = upper limit.
[c] von Montigny et al. 1995.

as $R \propto T^{-1.7}$, with $R_0 = 273$/per minute corresponding to $T_0 = 0.4$ TeV. The count rate is observed to be constant from the zenith out to an elevation of 55°. The rate-scaled threshold is cross-checked for consistency with the excess observed from the Crab Nebula, assuming a Crab integral spectrum of $N(>E) = 2.0 \times 10^{-11} T^{-1.4}$. The effective area is also determined from simulations. Both the energy threshold and effective area are currently subject to a 50% systematic error which should be reduced when more simulations and absolute calibrations are completed.

A number of changes were made in the camera and telescope during the period of these observations. Because of chubasco weather conditions in the summer in southern Arizona, there are generally no observations taken in August. This provides a convenient division between observing seasons since, in general, system changes are made during this summer interval. We define an "observing season" to span September to July. Because the system was still under development, the camera sensitivity varied each season, and hence it is most meaningful to consider each season separately. The description of the instrument condition for each of the seasons for which results are presented in this paper are summarized in Table 2.

3.3. *Observing Mode*

Observations were made in the usual ON/OFF mode with the source centered in the field of view during the ON observations; the OFF observations were made over an identical range of elevation and azimuth angles under clear skies. However, during much of the 1993–1994 observing season observations were made in the tracking mode with the OFF or control observations derived from the orientation of the images within the field of view (see below).

Table 3 is a summary of the observation log; the sources observed are listed together with the epoch of the observations, the actual number of minutes spent on source, the average elevation, and the observing mode used.

4. DATA ANALYSIS

4.1. *Supercuts*

As mentioned above, the hardware trigger introduces some discrimination against the larger, more diffuse, images from hadronic showers. Off-line in software the gamma-ray images are further discriminated from the much larger flux of cosmic-ray images by virtue of their narrower images (another 97.7% rejection) and by the fact that when they originate from a discrete source they tend to point toward the point of origin, usually the center of the camera (Hillas 1985).

This camera (with $N = 2$, $p = 40$, and gate width = 25 ns) was used to detect the Crab Nebula at a significance of 20 σ using the single parameter "azwidth" in 30 hr of on-source data taken in 1988–1989 (Vacanti et al. 1991). This data set was then used to determine an optimized, multiparameter set of cuts ("Supercuts") which yielded an (a posteriori) significance of 34 σ (Reynolds et al. 1993).

The overall (hardware and software selected) rejection of the charged cosmic-ray component within the field of view of the detector at the same energy threshold as the gamma-ray energy threshold was 99.96% within the 3° full field (determined from the independent 1989–1991 Crab data set [Reynolds et al. 1993]). The efficiency of registration of gamma rays was 60%. The angular resolution for individual gamma rays was 0°.15, and the location capability was 0°.1 (Akerlof et al. 1991). Both the collection area and the angular resolution pertain at the effective energy threshold, which is determined using the method previously outlined (Weekes 1976). The effective energy threshold and collection area (for Supercuts), determined from simulations, were 0.4 TeV and 3.5×10^8 cm^2, respectively, for this "standard" Crab database. The telescope trigger rate for this database was 273/per minute.

The Supercuts procedure depends on the source being centered in the field of view of the camera. This work includes two sources detected by EGRET (GRO J0431+29 and GRO J1837+59) which remain unidentified and whose positions are still uncertain. Because they are far from the Galactic plane, it is assumed that they are AGNs. One additional EGRET source, 2022−077, was originally classified as unidentified, and our data was collected at the best EGRET position, which differs from the AGN position by 0°.5. The positions that we used for these sources are listed in Table 4. Two limits are derived for the unidentified EGRET sources. One is based on the full Supercuts procedure, which is optimized for a source at the center of the field. The other is based only on the excess of narrow images ("shape" selection), with the selection based on images pointing toward the center of the camera ("orientation" selection) ignored; it is thus applicable when the source position is uncertain by as much as ±0°.5. The limit for 2022−077 is also derived in this way. Such a selection gives a slightly higher effective area than full Supercuts, but a much higher background level. The resultant limit is generally about a factor of 2 higher than that given by the full Supercuts procedure.

4.2. ON/OFF *Analysis*

For all the observations made prior to 1994 January the observing mode was the ON/OFF mode, in which equal time is spent observing the source and a comparison region which covers the same range of elevation and azimuth. After selection using the Supercuts procedure, a gamma-ray signal is readily apparent as a statistically significant excess in the ON compared with the OFF. The standard deviation was taken as $(\mathrm{ON}+\mathrm{OFF})^{1/2}$. For these observations, this simple form of the standard deviation gives essentially the same result as the maximum likelihood formula of Li & Ma (1983).

TABLE 2

CAMERA SETTINGS

Season	Threshold (photoelectrons)	Gate (ns)	Trigger	Collection Area (cm^2)	Energy (TeV)
1991–1992.....	50	30	1991 Feb	3.5×10^8	>0.5
1992–1993.....	36	30	1991 Mar	2.2×10^8	>0.35
1993–1994.....	30–40	25	1991 Feb	3.5×10^8	>0.30

TABLE 3

OBSERVATION LOG

Source	Epoch	ON Time (minutes)	Elevation	Observation Mode[a]
0116+319.....	1992 Sept–Oct	252	77°	O/O
	1994 Jan	181	67	T
0202+149.....	1994 Mar	57	55	T
0219+428.....	1993 Oct–Nov	251	71	O/O
0232−090.....	1992 Oct–Nov	252	49	O/O
0235+164.....	1994 Jan	89	67	T
0241+622.....	1992 Nov–1993 Jan	106	58	O/O
0316+413.....	1992 Sep	140	72	O/O
	1992 Dec	84	79	O/O
0415+379A.....	1992 Oct–Nov	225	71	O/O
0431+29	1993 Nov–Dec	84	70	O/O
0528+134.....	1992 Mar	56	51	O/O
	1994 Jan	348	69	T
0716+714.....	1992 Nov	130	50	O/O
	1994 Jan–Feb	416	50	T
0836+710.....	1992 Mar	140	43	O/O
	1992 Dec	84	50	O/O
	1994 Mar	58	50	T
0855+201.....	1993 Mar–Apr	194	72	O/O
	1994 Jan	379	73	T
1022+519.....	1994 Mar–Apr	151	69	T
1156+295.....	1994 Jan	117	82	T
1208+396.....	1993 Apr–May	196	74	O/O
1215+303.....	1993 Mar–Jun	188	65	O/O
1219+285.....	1993 Mar–Apr	140	68	O/O
	1994 Mar	235	78	T
1222+216.....	1994 Mar	76	70	O/O
	1994 Mar–May	229	74	T
1226+023.....	1992 Feb–Apr	84	56	O/O
	1993 Jan	78	56	O/O
	1994 Mar	201	58	T
1253−055.....	1991 Dec–1992 Apr	635	47	O/O
	1994 Apr–May	338	50	T
1353+388.....	1993 May	64	72	O/O
1400+162.....	1994 Feb–Mar	303	72	T
1514+072.....	1993 Mar–Apr	102	65	O/O
	1994 Apr–May	658	62	T
1604+159.....	1994 Mar	290	71	T
1633+382.....	1992 Apr	491	76	O/O
1652+398.....	1992 May–Jun	221	78	O/O
	1993 Apr	28	74	O/O
	1994 Apr	48	76	T
1720+309.....	1993 Apr	56	72	O/O
1727+502.....	1992 Jun–Jul	908	67	O/O
	1993 Apr	300	65	O/O
	1994 Apr	140	70	T
1837+59	1993 May–Jun	591	60	O/O
2022−077.....	1993 Jun	66	49	O/O
2200+420.....	1992 Jun–Jul	326	67	O/O
	1992 Oct	28	79	O/O
2230+114.....	1993 Oct–Nov	156	60	O/O
2251+58	1992 Sep	252	70	O/O
	1993 Oct–Nov	84	60	O/O
2304+04	1992 Oct	112	58	O/O
	1992 Nov	168	57	O/O

[a] O/O = ON/OFF; T = tracking.

TABLE 4

UNIDENTIFIED SOURCES: POINTING POSITIONS

Source	R.A. (1950.0)	Decl. (1950.0)
GRO J0431+29.....	$04^h26^m57^s$	+29°06′45″
GRO J1837+59.....	18 40 06	+58 48 24
2022−077.....	20 22 03	−08 15 15

4.3. *Tracking Analysis*

In 1994 January a new observation method was introduced which is more efficient and more sensitive. Basically it relies on the candidate gamma rays in the field of view of the ON observations to act as the control database, thus eliminating the need for OFF observations and ensuring that the control data are taken under identical atmospheric and camera conditions. In addition, the control data set (nonoriented images) is larger, and hence the standard deviation on the control data set is less.

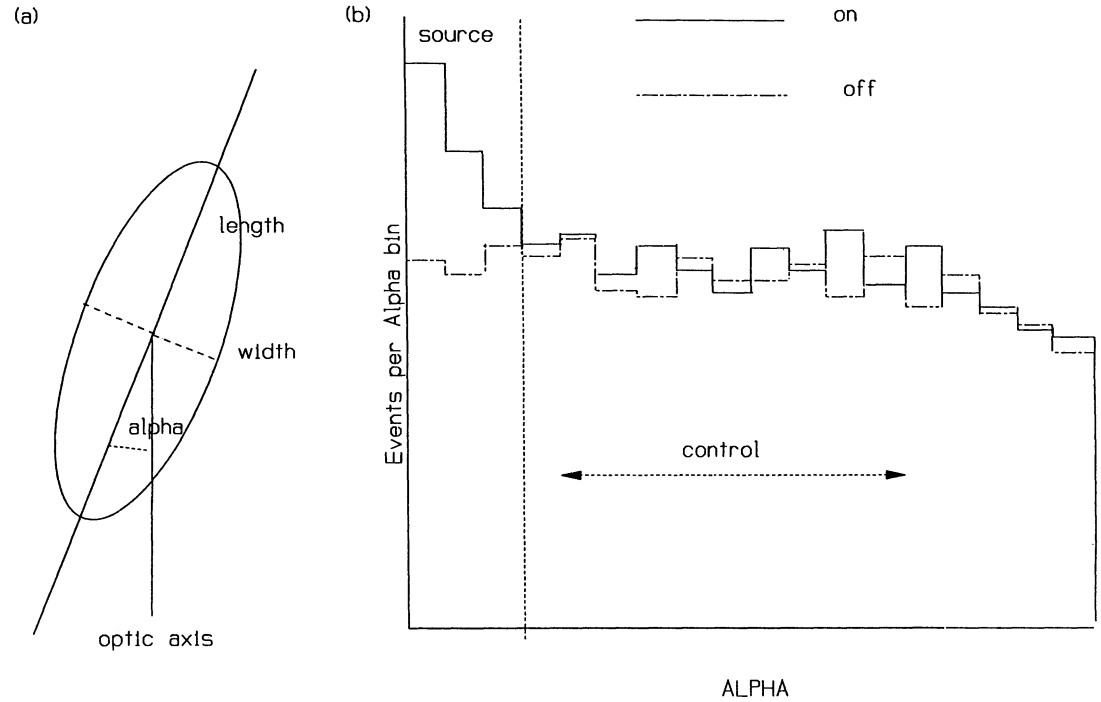

FIG. 1.—Alpha analysis: (*a*) definition of parameters; (*b*) Alpha plot showing ON and OFF data and defining the source (0°–15°) and control (20°–65°) regions

The method can be understood by reference to Figure 1. The image parameters are defined in Figure 1*a*; after selection by width and length, the events are plotted according to their orientation angle, α (Fig. 1*b*).

Under ideal conditions, the distribution with α is flat in the absence of a source; with a source present, simulations and observations of known sources, e.g., the Crab Nebula and Mrk 421, demonstrate that the source shows as an excess below 15°. If the field of view of the camera is less than 3°, edge effects cause some structure in the α distribution. The substitution of smaller pixel PMTs in the outer ring of the camera in 1993–1994 gave better angular resolution but reduced the field of view from 3°.9 to 3°.0. The distribution then exhibits a falloff beyond 75°. However, the form of the distribution (in the absence of a source) is constant, and a ratio can be derived for the ON to OFF α bins. Here we defined the ON region as 0°–15° and the OFF region as 20°–65°; the ratio k was then found empirically from a number of null source observations to be 0.335 ± 0.009. The standard deviation was taken as $[k(\mathrm{ON}+\mathrm{OFF})]^{1/2}$, where ON is the total number of events in the ON region, OFF is the total number of events in the OFF region, and k is the ratio of the number of bins in the ON region to the number of bins in the OFF region, which is 1/3 for this analysis. The standard deviation was calculated as in § 4.2.

Using this technique, flaring activity has been observed in Mrk 421; these observations have been reported elsewhere (Kerrick et al. 1995).

5. RESULTS

To check that the results of this analysis truly correspond to a normal distribution, the statistical significances from each run on all sources were compiled into histograms (Fig. 2). Chi-square distributions were then calculated to compare the histograms to a normal distribution of mean 0 and $\sigma = 1$ with bins of width 0.5 σ. All significances greater than 1.5 σ (or less than -1.5) were grouped into a single bin for purposes of χ^2 determination. Separate histograms were accumulated for the Shape only, Orientation only, and Supercuts excesses for ON/OFF pairs, and for significances computed using the tracking mode data (α analysis).

The chance probabilities of exceeding the calculated χ^2 values (7 degrees of freedom) are 0.0054, 0.034, 0.088, and 0.28 for Shape, Orientation, Supercuts, and Alpha, respectively. For the ON/OFF runs, separate histograms were accumulated for each observing season. Each season was compatible with the above results, except for the Shape distribution as noted below.

The low chance probability for the Shape-selected data is the result of an offset of the center of the distribution to positive values. This shift came from the 1991–1992 observing season data, where the mean shape excess was 0.375. This shift is not associated with a particular source or with some particularly strong runs; it could be interpreted as evidence for weak emission from a number of sources. However, this hypothesis is not verified in the Orientation or Supercuts selection. We note that the Shape analysis is most susceptible to systematic biases resulting from differences in the brightness of the sky in the ON and OFF regions.

Table 5 contains the list of significances of the ON/OFF effect for each source for the Supercuts and/or Alpha analysis. The α plots for the 18 sources observed in 1993–1994 are shown in Figure 3; there are no significant excesses in the gamma-ray domain.

We conclude that there are no statistically significant excesses for any of the sources. Upper limits have been calculated at the 99.9% significance level using the method of Helene (1983). Table 5 lists the epoch and energy threshold of each observation, along with the limiting values of both the excess number of counts from the source, and the flux, which is the upper limit of counts divided by the observation time and

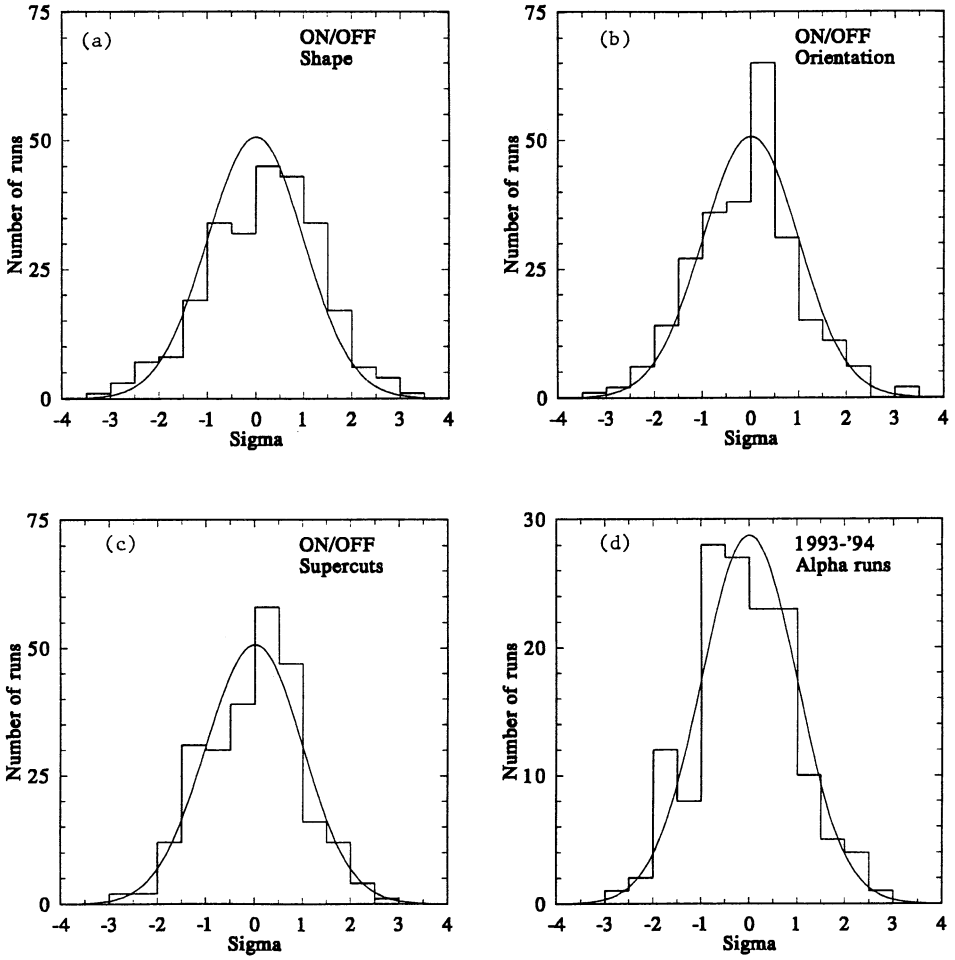

FIG. 2.—Distribution of significances for sources observed in 1993–1994: selection by (*a*) Shape; (*b*) Orientation; (*c*) Supercuts (Shape and Orientation); (*d*) Alpha analysis.

the effective area of the detector. The confidence level was chosen to correspond roughly to the 3 σ level, which would be the minimum level acceptable for claiming a source detection. In view of the reported variability of these objects, it is important to emphasize that these limits pertain only for the limited epoch of the observations.

During this same observing period, observations were interspersed with observations of the Crab Nebula and Mrk 421. All the observing innovations discussed above were tested on these sources which were consistently detected over these three seasons of observation. In a separate paper (Schubnell et al. 1995), the results of observations on Mrk 421 over the epoch 1992–1994 are reported. The integral fluxes recorded during these observations were as follows: 1991/1992, $1.59 \pm 0.20 \times 10^{-11}$ cm^{-2} s^{-1} (>500 GeV); 1992/1993, $1.47 \pm 0.30 \times 10^{-11}$ cm^{-2} s^{-1} (>500 GeV); and 1993/1994, $1.18 \pm 0.20 \times 10^{-11}$ cm^{-2} s^{-1} (>350 GeV) (preburst).

Upper limits on the gamma-ray emission from EGRET-detected AGNs have been reported at higher energies by the Tibet Air Shower Array (Amenomori et al. 1994), by the Cygnus group (Alexandreas et al. 1993), and by the CASA-MIA experiment (Catanese et al. 1994). The results reported here are the first comprehensive set of observations at energies between 100 and 1000 GeV and are the most serious limitation on the energy spectrum beyond the upper limit of the EGRET experiment.

The high-energy gamma-ray spectrum of several of the EGRET-detected sources for which energy spectra have been published are plotted in Figure 4 together with upper limits from the air shower experiments and the upper limits reported here.

6. DISCUSSION

The observations reported here were undertaken to test the hypothesis that some or all of the EGRET-detected AGNs had detectable components in the TeV energy region. With the exception of Mrk 421, none of the 15 AGNs detected by EGRET which were included in this observing program were detected. Since the observation of Mrk 421 shows that for flat spectrum sources the Whipple telescope is more sensitive than EGRET, the search was extended to objects with somewhat similar properties to Mrk 421 but which were not detected by EGRET; again, no emission was detected. The conclusions from these null results are restricted by the fact that almost all the AGNs detected by EGRET are time variable (as is Mrk 421 at TeV energies; Kerrick et al. 1995). However, a reasonable conclusion is that the observable spectrum of AGNs shows a steepening between 10 GeV and 300 GeV. Such

TABLE 5

AGN UPPER LIMITS

Source	Epoch	Threshold (TeV)	ON (Number of events)	OFF (Number of events)	σ	Counts	Flux ($> \times 10^{-12}$ cm^{-2} s^{-1})
0116+319	1992 Sep–Oct	0.45	132	121	+0.7	62	19
	1994 Jan[a]	0.3	240	774	−1.0	48	13
0202+149	1994 Mar[a]	0.35	123	387	−0.5	38	32
0219+428	1993 Oct–Nov	0.35	358	343	+0.6	100	19
0232−090	1992 Oct–Nov	0.45	449	448	+0.0	99	30
0235+164	1994 Jan[a]	0.3	144	423	+0.2	48	25
0241+622	1992 Nov–1993 Jan	0.4	239	218	+1.0	88	63
0316+413	1992 Sep	0.5	65	59	+0.5	41	14
	1992 Dec	0.35	212	218	−0.3	64	57
0415+379A	1992 Oct–Nov	0.45	270	291	−0.9	63	21
J0431+29 (Shape)	1993 Nov–Dec	0.3	143	121	+1.4	73	41
			757	794	−0.9	104	53
0528+134	1992 Mar	0.5	59	75	−1.4	28	24
	1994 Jan[a]	0.3	630	1884	+0.1	97	13
0716+714	1992 Nov	0.45	183	177	+0.3	67	39
	1994 Jan–Feb[a]	0.35	1071	3213	+0.0	124	14
0836+710	1992 Mar	0.6	260	253	+0.3	80	27
	1992 Dec	0.4	177	179	−0.1	61	55
	1994 Mar[a]	0.35	153	432	+0.6	54	44
0855+201	1993 Mar–Apr	0.3	159	171	−0.7	51	20
	1994 Jan[a]	0.3	498	1575	−1.0	68	8.6
1022+519	1994 Mar–Apr[a]	0.3	213	603	+0.7	64	20
1156+295	1994 Jan[a]	0.3	114	395	−0.2	38	15
1208+396	1993 Apr–May	0.3	172	158	+0.8	72	28
1215+303	1993 Mar–Jun	0.3	196	170	+1.4	86	34
1219+285	1993 Mar–Apr	0.3	102	108	−0.4	43	23
	1994 Mar[a]	0.3	348	1062	−0.3	67	14
1222+216	1994 Mar	0.3	113	109	+0.3	52	33
	1994 Mar–May[a]	0.3	327	1035	−0.8	57	12
1226+023	1992 Feb–Apr	0.55	63	71	−0.7	32	18
	1993 Jan	0.35	176	175	+0.1	62	61
	1994 Mar[a]	0.3	399	1251	−0.8	65	15
1253−055	1991 Dec–1992 Apr	0.55	573	562	+0.3	120	9.0
	1994 Apr–May[a]	0.3	1254	3681	+0.7	156	22
1353+388	1993 May	0.3	66	62	+0.4	41	48
1400+162	1994 Feb–Mar[a]	0.3	510	1575	−0.6	76	12
1514+072	1993 Mar–Apr	0.3	87	113	−1.8	30	23
	1994 Mar[a]	0.3	1425	4203	+0.6	162	12
1604+159	1994 Mar[a]	0.3	411	1305	−1.0	62	10
1633+382	1992 Apr	0.5	104	133	−1.9	33	3.2
1652+398	1992 May–Jun	0.55	67	67	+0.0	38	8.2
	1993 Apr	0.35	16	11	+1.0	21	58
	1994 Apr[a]	0.3	84	216	+1.2	43	43
1720+309	1993 Apr	0.3	33	34	−0.1	26	35
1727+502	1992 Jun–Jul	0.5	407	362	+1.6	131	6.9
	1993 Apr	0.35	153	162	−0.5	52	13
	1994 Apr[a]	0.3	237	711	+0.0	59	20
J1837+59 (Shape)	1993 May–June	0.3	668	715	−1.3	91	12
			3705	3818	−1.3	210	24
2022+077 (Shape)	1993 Jun	0.35	142	147	−0.3	52	60
			857	783	+1.8	200	200
2200+420	1992 Jun–Jul	0.5	132	147	−0.9	45	6.5
	1992 Oct	0.45	33	24	+1.2	33	88
2230+114	1993 Oct–Nov	0.35	320	366	−1.8	58	18
2251+158	1992 Sep	0.5	106	111	−0.3	45	8.4
	1993 Oct–Nov	0.35	143	145	−0.1	54	31
2304+042	1992 Oct	0.45	118	132	−0.9	42	29
	1992 Nov	0.4	220	215	+0.2	73	33

[a] Alpha analysis for tracking runs.

a steepening could have three origins: (i) an inherent steepening in the particle acceleration spectrum in the AGN or in the gamma-ray production spectrum; (ii) absorption of the gamma rays close to the AGN; (iii) absorption of gamma rays in intergalactic space. For very high energy gamma rays, the dominant absorption process is pair production on infrared photons (Nikishov 1962; Ginzburg & Syrovatskii 1964; Gould & Schreder 1967); this effect has recently been revisited for absorption on intergalactic infrared photons (Stecker, de Jager, & Salamon 1992; Dwek & Slavin 1994; MacMinn & Primack 1995; Biller et al. 1995).

The observation of the cutoff in the gamma-ray spectrum of AGNs may be used to differentiate between models of the origin of the gamma-ray emission; this is still the subject of

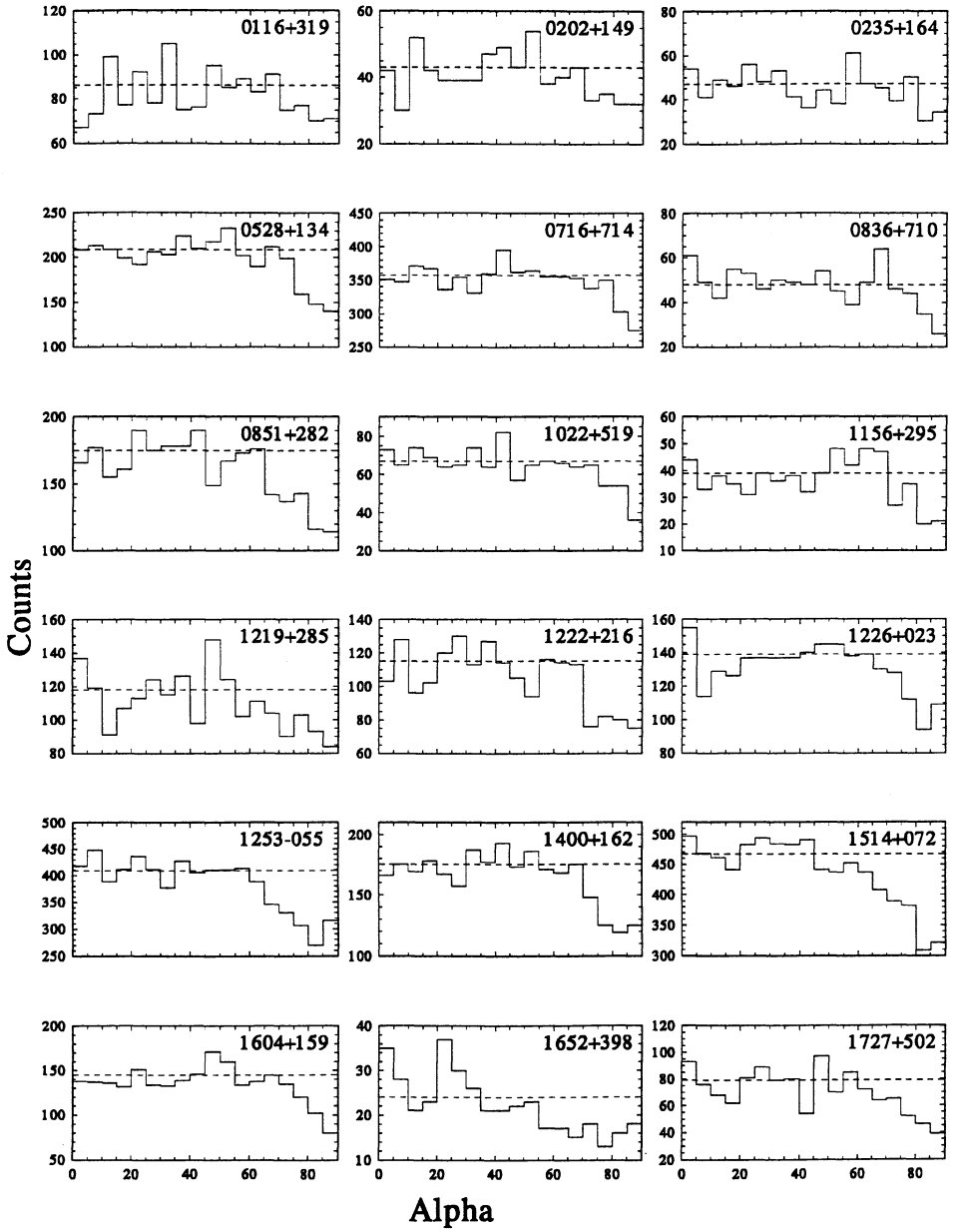

FIG. 3.—Alpha plots for 18 sources observed in 1993–1994

much theoretical debate which is well summarized in von Montigny et al. (1995). In the lepton models, the emission from blazars involves inverse Compton scattering of lower energy target photons by relativistic electrons in the inner region of the jet. Some of these models predict a cutoff in the energy range 10–100 GeV (e.g., Sikora, Begelman, & Rees 1994). In general, these inverse Compton spectrum models have difficulty explaining TeV emission because of the break at the Klein-Nishina region. The model by Zdziarski & Krolik (1993) circumvents this limitation. On the other hand, hadronic models (Mannheim & Biermann 1992) explain the gamma-ray emission as pion decay from hadron-hadron interactions; it is easier to explain a hard spectrum out to TeV energies in these models, but in at least one, the spectrum should cutoff sharply above 10 GeV (Mannheim 1993). Sensitive observations in the 10–100 GeV region may be crucial to differentiate between these models, but there are currently no viable experiments working in this energy range.

The observations of a consistent gamma-ray component that extends to at least 1 TeV would be a major constraint on all these models; if Mrk 421 is typical, then such emission may be inherent, and the failure to detect a signal from these other AGNs may be the result of absorption. It may be significant that the absolute luminosity of Mrk 421 is less than most of the other AGNs detected by EGRET, and hence the local infrared fields that might absorb the TeV gamma rays via pair production will be less intense.

For the nearer AGNs ($z < 0.1$), the effects of intergalactic absorption are expected to be small in the range 100 GeV to 10 TeV; for more distant objects, the amount of absorption may be considerable but can be calculated if the intergalactic infrared density as a function of redshift were known. However,

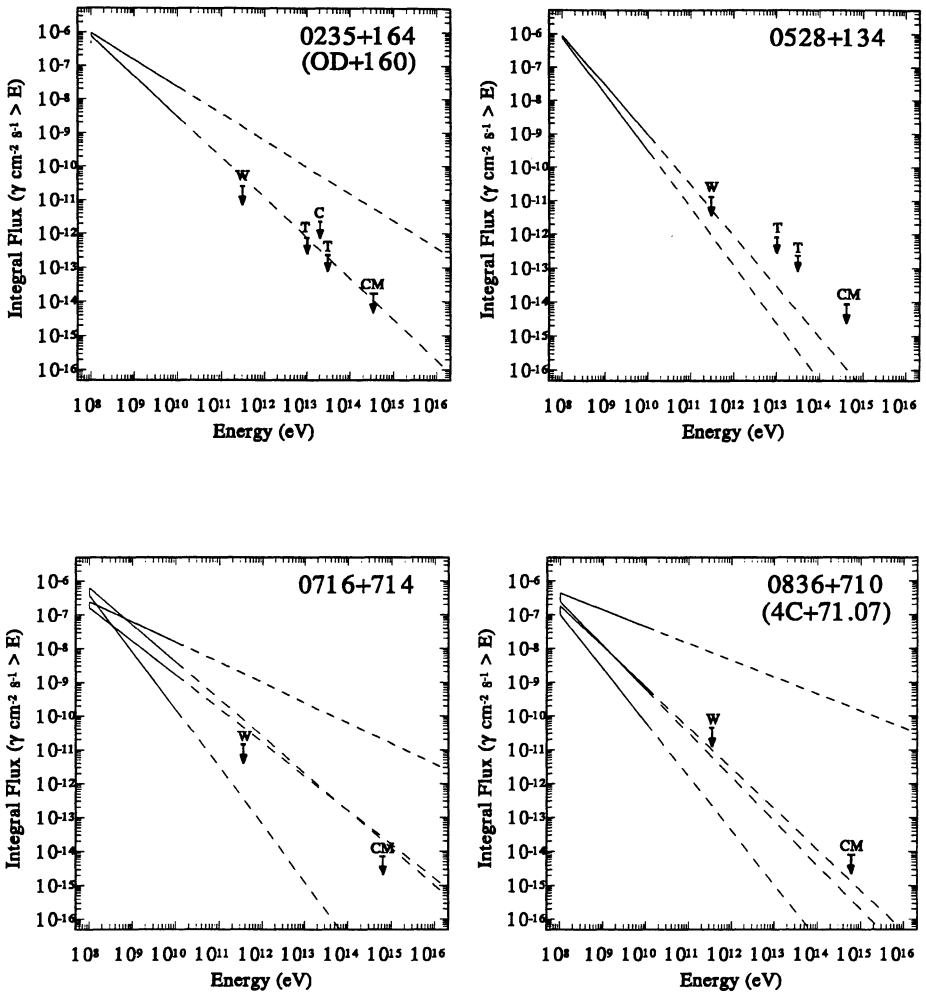

FIG. 4a

FIG. 4.—Energy spectra for (*a*) 0235+164 (OD +160), 0528+134, 0716+714, and 0830+710; (*b*) 1226+023 (3C 273), 1253−055 (3C 279), 1633+382, 2022−077 (NRAO 62); (*c*) 2251+158 (3C 454.3), 2330+114 (CTA 102). T = Tibet Air Shower Array (Amenomori et al.1994); C = Cygnus experiment (Alexandreas et al. 1993); CM = CASA-MIA (Catanese et al. 1994); W = Whipple (this paper). Limits for the Tibet and CASA-MIA experiments are derived directly, whereas the Cygnus experiment was corrected for intergalactic absorption on the microwave background. Solid lines are the limits of the spectra measured by the EGRET experiment (Fichtel et al. 1994), and dashed lines are their extrapolation to higher energies.

there is considerable uncertainty in even the local value of this quantity which is difficult to measure directly. We have recently used the detection of Mrk 421 to deduce limits on the infrared density (Biller et al. 1995; see also De Jager, Salamon, & Stecker 1994; Dwek & Slavin 1994).

The detection of TeV signals from a number of AGNs at a variety of distances could enable the intergalactic starlight density to be determined, provided there was some consistency in the emission spectra of the various AGNs. Since the absorption curve would be quite distinctive (if the effect of galactic evolution on the infrared background was known), its detection would be another strong argument in favor of AGNs lying at distances indicated by their redshift assuming the Hubble expansion velocity. It has been shown that the intergalactic infrared photon density is strongly dependent on the epoch of galaxy formation (MacMinn & Primack 1995).

It has also been suggested that if the intergalactic infrared density were known, then the measured absorption could be used to measure the Hubble constant (Salamon, Stecker, & De Jager 1994). However, it is dangerous to infer too much from the detection of a single TeV-emitting AGN.

We acknowledge the assistance of Kevin Harris in the observing program. Research in gamma-ray astronomy of the Whipple Collaboration is supported by the US Department of Energy, by NASA, by the Smithsonian Scholarly Studies Fund, by the PPARC of Great Britain, and by Eolas, the Irish funding agency. We acknowledge use of the NASA/IPAC Extragalactic Database (NED) maintained by the California Institute of Technology.

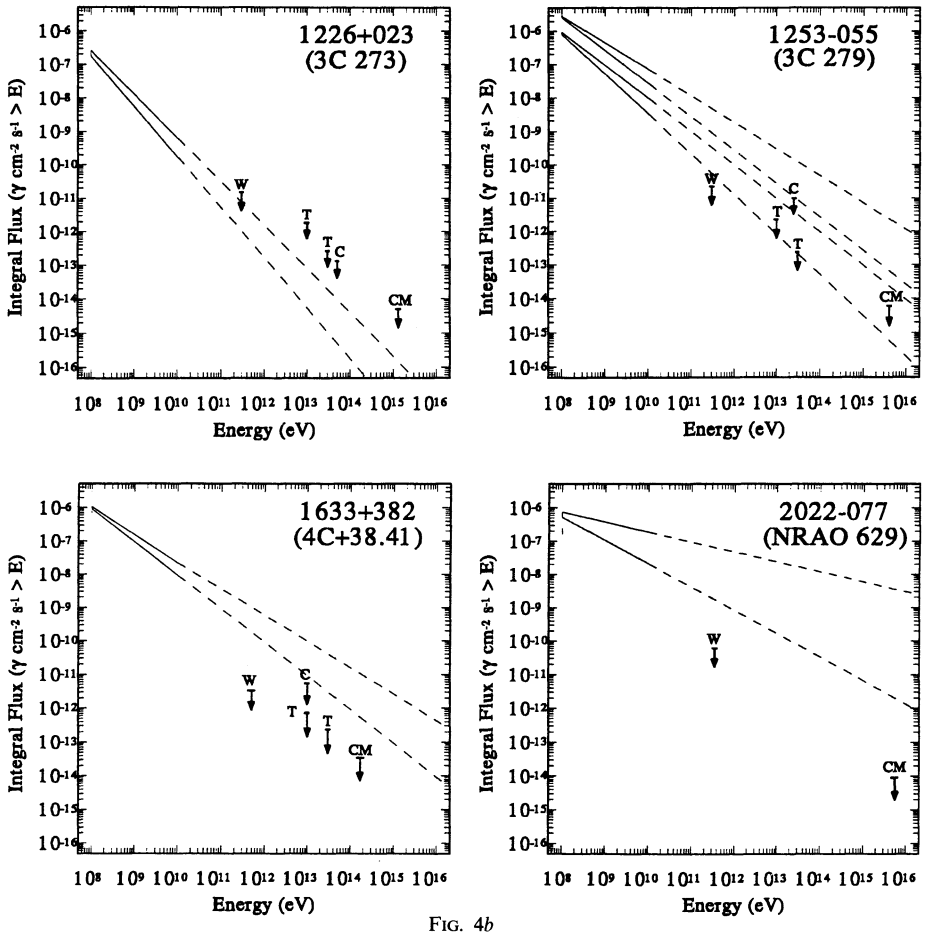

FIG. 4*b*

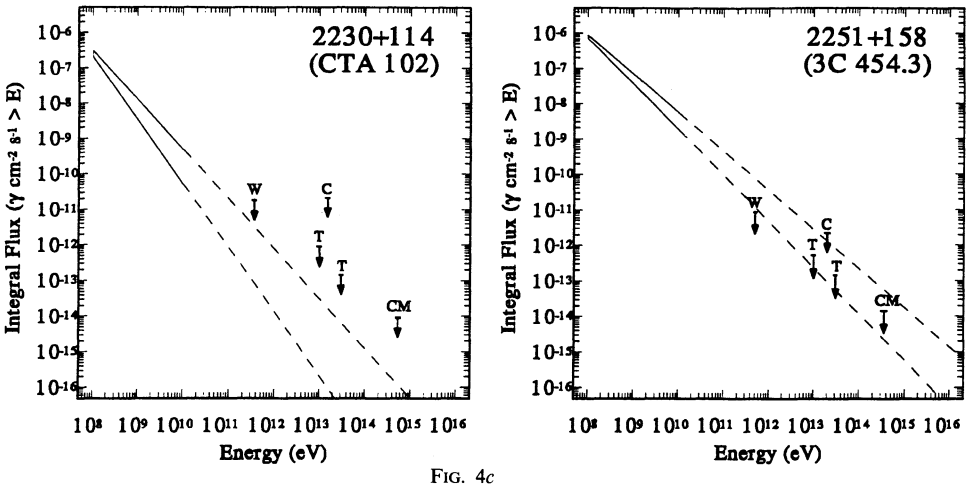

FIG. 4*c*

REFERENCES

Akerlof, C. W., et al. 1991, ApJ, 377, L97
Alexandreas, D. E., et al. 1993, ApJ, 418, 832
Amenomori, M., et al. 1994, ApJ, 429, 634
Biller, S. D., et al. 1995, ApJ, 445, 227
Catanese, M., et al. 1994, in AIP Conf. Proc., Div. of Part. and Fields Meeting, in press
Cawley, M. F., et al. 1985, Proc. 19th Int. Cosmic-Ray Conf. (La Jolla), 1, 264
———. 1990, Exp. Astron., 1, 185
Cawley, M. F., & Weekes, T. C. 1995, Exp. Astron., in press.
Fichtel, C. A., et al. 1994, ApJS, 94, 551
de Jager, O. C., Salamon, M. H., & Stecker, F. W. 1994, Nature, 369, 294
Dwek, E., & Slavin, J. 1994, ApJ, 436, 696
Ginzburg, V. L., & Syrovatskii, S. I. 1964, Soviet Phys.-JETP, 18, 245
Gould, R. J., & Schreder, G. P. 1967, Phys. Rev., 155, 1404
Grindlay, J. E., et al. 1975, ApJ, 197, L9
Hartman, R. C., et al. 1992, ApJ, 385, L1
Helene, O. 1983, Nucl. Instrum. Methods Phys. Res., 212, 319
Hillas, A. M. 1985, Proc. 19th Int. Cosmic-Ray Conf. (La Jolla), 3, 445

Kerrick, A. D., et al. 1995, ApJ, 438, L59
Li, T-P., & Ma, Y. Q. 1983, ApJ, 272, 317
Long, C. D., et al. 1965, Proc. 9th Int. Cosmic-Ray Conf. (London), 1, 318
MacMinn, D., & Primack, J. 1995, ApJ, submitted
Mannheim, K. 1993, A&A, 269, 67
Mannheim, K., & Biermann, P. L. 1992, A&A, 53, L21
Nikishov, A. I. 1962, Soviet Phys.–JETP, 14, 393
Punch, M., et al. 1992, Nature, 160, 477
Reynolds, P. T., et al. 1993, ApJ, 404, 206
Salamon, M. H., Stecker, F. W., & de Jager, O. C. 1994, ApJ, 423, L1
Schubnell, M. S., et al. 1995, ApJ, submitted.
Sikora, M., Begelman, M. C., & Rees, M. J. 1994, ApJ, 421, 153
Stecker, F. W., de Jager, O. C., & Salamon, M. H. 1993, ApJ, 415, L71
Stepanian, A. A., et al. 1975, Ap&SS, 38, 267
Vacanti, G., et al. 1991, ApJ, 377, 467
von Montigny, C., et al. 1995, ApJ, 440, 525
Weekes, T. C. 1973, Proc. 13th Int. Cosmic-Ray Conf. (Denver), 1, 446
———. 1976, Nuovo Cimento, 35B, 95
Weekes, T. C., et al. 1972, ApJ, 174, 165
Zdziarski, A. A., & Krolik, J. H. 1993, ApJ, 409, L33

Note added in proof.—Mrk 501 (1652+398) has subsequently been detected at TeV energies at a level below the upper limits reported here (J. Quinn et al., IAU Circ., 6178 [1995]).